

Direct Numerical Demonstration of Sign-preserving Quasiparticle Interference via Impurity inside Vortex Core in Unconventional Superconductors

Yuki Nagai, Noriyuki Nakai, and Masahiko Machida

*CCSE, Japan Atomic Energy Agency, 6-9-3 Higashi-Ueno, Tokyo 110-0015, Japan and
CREST(JST), 4-1-8 Honcho, Kawaguchi, Saitama, 332-0012, Japan*

(Dated: November 29, 2018)

We perform large-scale numerical calculations self-consistently solving the Bogoliubov-de Gennes (BdG) equations in the magnetic field together with random impurities to directly demonstrate the typical quasi-particle interference (QPI) in the presence of vortices as observed by scanning tunneling microscopy/spectroscopy experiments in unconventional superconductors. The calculations reveal that vortex itself never works as a scatter causing the QPI pattern but vortex core containing impurity brings about the enhancement of the sign-preserving QPI peaks. Its origin is Andreev bound-states distorted by impurity, and all the measurement findings are consistently explained by the scenario based on the numerical results.

PACS numbers: 74.20.Rp, 74.25.Op, 73.22.-f

I. INTRODUCTION

Since the discovery of High-Tc cuprate superconductors, the pairing mechanism has been a central issue in condensed matter physics over two decades. The superconducting gap symmetry was one of the most important clues to identify the mechanism. Historically, the symmetry in High-Tc cuprate superconductors was proven to be *d*-wave by a direct observation of the half-fluxon in the tri-crystal junction and supported by other measurements¹. Recently, a new type of symmetry, i.e., the sign-reversing *s*-wave pairing symmetry has been proposed as a candidate in brand-new iron-based High-Tc superconductors.

The measurement of quasi-particle interference (QPI) patterns by the scanning tunneling microscopy/spectroscopy (STM/STS) is now listed as a powerful tool directly probing the pairing symmetry³⁻⁹. The QPI pattern is obtained by Fourier-transforming the ratio $Z(\mathbf{r}, V) = g(\mathbf{r}, V)/g(\mathbf{r}, -V)$ of the conductance maps $g(\mathbf{r}, V) = dI/dV(\mathbf{r}, V)$ for the position \mathbf{r} and the bias voltage $\pm V$. So far, it has been widely accepted that a relative sign difference inside superconducting order parameter can be directly detected by the magnetic field dependence of its Fourier transformation $|Z(\mathbf{q}, \omega)|$. The reason is that if a vortex works as a magnetic impurity then the number of magnetic impurities increases with increasing the magnetic field and the sign-preserving scattering⁵ dominates over the sign-reversing one. However, it is just an intuitive idea, and there is no direct theoretical confirmation except for an indirect support through a perturbative approach⁹. Generally, vortex breaks the translational symmetry and makes low-energy Andreev bound states inside the core. Thus, the vortex is never a simple impurity and beyond the reach of any perturbative approaches. In iron-based superconductors, the QPI experimental result² is presently regarded as one of a few crucial facts supporting the sign-reversing *s*-wave symmetry. We have to rush to confirm the intuitive assumption.

In this paper, we therefore investigate QPI in the presence of vortices through a direct numerical calculation on the self-consistent BdG equations. A main finding of the present paper is that vortex works as a scatter breaking the time-reversal symmetry only when impurity is captured by the core. Thus, this finding indicates that vortex pinning, i.e., so-called the core pinning is crucial in supporting the previous QPI scenario in the magnetic field.

To numerically obtain the QPI map, we need to perform a large-scale calculation in real-space, since the QPI map is obtained by Fourier transforming a sufficiently wide real-space data. However, the computer resource to numerically solve the BdG equations becomes too huge, as long as one employs the conventional Hamiltonian-matrix diagonalization-scheme whose computational cost increases in N^3 manner, where N is the number of grid points in real-space. In this paper, we instead implement the Chebyshev-polynomial expansion scheme¹⁵⁻¹⁷ as a self-consistent solver of the BdG equations¹⁸. We stress that the present real-space area is wider than 10-nm scale square, which is much beyond the conventional size.

II. MODEL AND METHOD

The target tight-binding model Hamiltonian $\mathcal{H} = \mathcal{H}_{\text{BCS}} + \mathcal{H}_{\text{imp}}$. Here, BCS Hamiltonian, $\mathcal{H}_{\text{BCS}} = -\sum_{ij,\sigma} (\tilde{t}_{ij} + \mu \delta_{ij}) c_{i\sigma}^\dagger c_{j\sigma} + \sum_{ij} [\Delta_{ij} c_{i\uparrow}^\dagger c_{j\downarrow}^\dagger + \text{h.c.}]$, where $c_{i\sigma}^\dagger$ creates an electron with spin σ at site i and μ denotes the chemical potential. The hopping integrals \tilde{t}_{ij} include the Peierls phase factor $\tilde{t}_{ij} = t_{ij} \exp \left[i \frac{\pi}{\phi_0} \int_{\mathbf{r}_i}^{\mathbf{r}_j} \mathbf{A}(\mathbf{r}) \cdot d\mathbf{r} \right]$ in the presence of the magnetic field, where $\mathbf{A}(\mathbf{r})$ is the vector potential and $\phi_0 = hc/2e$ is the flux quantum. The impurity part of the Hamiltonian can be written as $\mathcal{H}_{\text{imp}} = \sum_{i,\sigma} V_i^{\text{imp}} c_{i\sigma}^\dagger c_{i\sigma}$. One diagonalizes \mathcal{H} to solve

the BdG equations written as

$$\sum_j \begin{pmatrix} \hat{K}_{i,j} & \hat{\Delta}_{i,j} \\ \hat{\Delta}_{i,j}^* & -\hat{K}_{i,j}^* \end{pmatrix} \begin{pmatrix} u_\alpha(\mathbf{r}_j) \\ v_\alpha(\mathbf{r}_j) \end{pmatrix} = E_\alpha \begin{pmatrix} u_\alpha(\mathbf{r}_i) \\ v_\alpha(\mathbf{r}_i) \end{pmatrix}. \quad (1)$$

Here, $K_{i,j} = -t_{ij} - (\mu - V_i^{\text{imp}})\delta_{ij}$, and $\Delta_{i,j} = \Delta(\mathbf{r}_i, \mathbf{r}_j) = V_{ij} \sum_\alpha^{2N} u_\alpha(\mathbf{r}_j) v_\alpha^*(\mathbf{r}_i) f(E_\alpha)$, where N is the number of the lattice sites, V_{ij} denotes the pairing interaction, and $f(x)$ is the Fermi distribution function. In this paper, the hopping is restricted only in the nearest neighbor ($t_{ij} = t$) for simplicity. The chemical potential $\mu = -1.5t$, and the pairing interaction is given only on the link of the nearest neighbor, $V_{ij} = V = -2.2t$. We self-consistently calculate $d_{x^2-y^2}$ -wave order parameter, $\Delta_d(\mathbf{r}_i) = V(\Delta_{\hat{x},i} + \Delta_{-\hat{x},i} - \Delta_{\hat{y},i} - \Delta_{-\hat{y},i})/4$ with $\Delta_{\pm\hat{e},i} = \Delta(\mathbf{r}_i, \mathbf{r}_i \pm \hat{e}) \exp \left[i \frac{\pi}{\phi_0} \int_{\mathbf{r}_i}^{(\mathbf{r}_i + \mathbf{r}_i \pm \hat{e})/2} \mathbf{A}(\mathbf{r}) \cdot d\mathbf{r} \right]^{19}$, where \hat{x} and \hat{y} denote the unit vectors in a square lattice.

Let us briefly show how to solve self-consistently the BdG equations (1) including the gap equation with use of the Chebyshev-polynomial expansion scheme. The mean-field can be expressed as $\langle c_i c_j \rangle = -\frac{1}{2\pi i} \int_{-\infty}^{\infty} d\omega f(\omega) \vec{e}(j)^T \hat{d}(\omega) \vec{h}(i)$, where $[\vec{e}(i)]_\gamma = \delta_{i,\gamma}$, and $[\vec{h}(i)]_\gamma = \delta_{i+N,\gamma}$. The spectral density $\hat{d}(\omega)$ is given by $\hat{G}^R(\omega) - \hat{G}^A(\omega)$ whose Dirac's delta functions are expanded by a series of Chebyshev-polynomials¹⁸. Then, one can rewrite the gap equation at zero-temperature as

$$\Delta(\mathbf{r}_i, \mathbf{r}_j) = -\frac{2V_{ij}}{\pi} \sum_{n=1}^{n_c} \vec{e}(j)^T \vec{h}_n(i) \frac{\sin[n \arccos(-b/a)]}{n}, \quad (2)$$

where n is the order of the Chebyshev-polynomial, and n_c denotes a cutoff parameter. $\vec{h}_n(i)$ is calculated by the recurrence formula, $\vec{h}_{n+1}(i) = 2(\mathcal{H} - \hat{1}b)/a\vec{h}_n(i) - \vec{h}_{n-1}(i)$ and $\vec{h}_0(i) = \vec{h}(i)$ and $\vec{h}_1(i) = 2(\mathcal{H} - \hat{1}b)/a\vec{h}(i)$, where the renormalized factors a and b are set in the order of the band-width, e.g., $b = -\mu$, respectively. We point out that calculation results are insensitive to choice of these parameters^{17,18}. This drastically reduces the self-consistent calculation costs since the calculation algorithm is perfectly free from the use of any diagonalization scheme. We always set $n_c = 1000$ through the present calculations, which is confirmed to be enough¹⁸. Since each grid point is completely independent in the vector formula, we can efficiently solve these equations by using parallel multi-core computers.

The calculation target is 160×160 square lattice, which conventionally requires a full diagonalization of 51200×51200 matrix. If the lattice constant $\sim \text{\AA}$, then its real-scale area is beyond 10 nm square. In this case, it is a quite hard task for the conventional diagonalization scheme to self-consistently solve the problem, while the present scheme can finish the self-consistent calculation during about 10 minutes when using 128 cores.

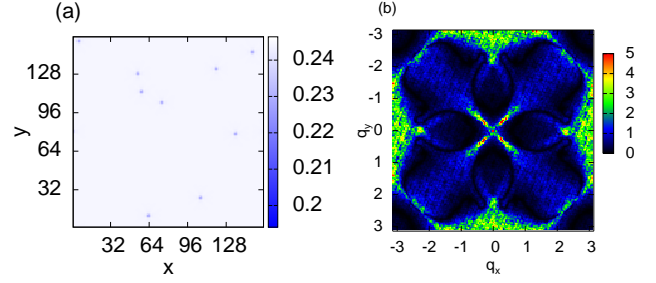


FIG. 1. (Color online) (a): A spatial profile of the $d_{x^2-y^2}$ -wave order-parameter amplitude $|\Delta_d(\mathbf{r}_i)|$. (b): A \mathbf{q} -space profile of $Z(\mathbf{q}, E)$, which is obtained by Fourier transforming the quantity $Z(\mathbf{r}, \omega) \equiv N(\mathbf{r}, \omega)/N(\mathbf{r}, -\omega)$ at the energy $\omega = 0.04t$. The system size is 160×160 square grids with 10 randomly distributed impurities without vortex.

III. RESULTS

Here, let us show how to demonstrate that QPI in the presence of the magnetic field actually detects the sign-preserving quasi-particle scattering. First, we examine the quasi-particle scattering by non-magnetic impurities without vortices. Second, we study QPI for a vortex lattice without any impurities to know whether vortex works as a magnetic impurity. Third and fourth, we investigate two vortex systems with random impurities. In the third case, all impurities are away from any vortex cores. On the other hand, one impurity locates inside the vortex core in the forth case. Through the comparison between the third and fourth cases, we find that impurity locating inside the vortex core is essential to identify the relative phase difference of the superconducting order parameter.

At first, let us examine the QPI with no vortex. We introduce randomly-distributed impurities as $V_i^{\text{imp}} = 0.3t\delta(\mathbf{r} - \mathbf{r}^{\text{imp},i})$ ($i = 1, \dots, 10$). As shown in Fig. 1(a), the order parameter amplitude $|\Delta_d(\mathbf{r}_i)|$ shows relatively small values only around the impurity sites. In this case, as seen in Fig.1(b), the quantity $Z(\mathbf{q}, E)$, i.e., the Fourier transformation of $Z(\mathbf{r}, \omega) (\equiv N(\mathbf{r}, \omega)/N(\mathbf{r}, -\omega))$ is equivalent to those in the previous theoretical studies using the diagrammatic approach⁹. This map is regarded as a typical QPI pattern, which clearly reflects the scattering feature of quasi-particles on the Fermi surface (see the left panel of Fig.4 for the present Fermi surface).

Second, we study a vortex lattice without any impurities. According to the standard way introducing vortices^{14,19}, we make a square vortex lattice, whose unit vector is in the direction of 45° from a -axis of the original tight-binding model (see the inset of Fig. 2). Then, the local density of states (LDOS), $N(r, E)$ is calculated and the gap edge is found to be $\sim 0.25t$ as seen in the left panel of Fig. 2. The QPI map is displayed in the right panel of Fig. 2, where we note that the map is irrelevant to QPI. Namely, one can not find out any characteristic

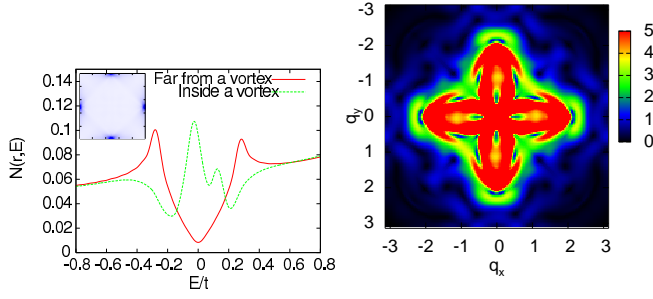


FIG. 2. (Color online) Left panel: Local densities of states far from a vortex core and inside a vortex core without any impurities. Inset: A spatial profile of the $d_{x^2-y^2}$ -wave order-parameter amplitude $|\Delta_d(\mathbf{r}_i)|$. Right panel: A \mathbf{q} -space profile of $Z(\mathbf{q}, E)$. For the definition $Z(\mathbf{q}, E)$ and the system size, see the caption of Fig. 1.

wave-vector peaks arising from the impurity scattering in contrast to Fig. 1. In the case, Andreev bound states inside the vortex core just produce such a pattern only around $q \sim 0$. Thus, it is found that vortex can not be regarded as a magnetic impurity scatter.

Now, let us introduce random impurities into the vortex lattice. As the third case, 10 impurities are randomly distributed, but all impurities are away from any vortex cores. In this case, their impurity potential is not so deep and their density is so dilute that the vortex lattice is not almost distorted compared to the case without impurities. Such a situation is called "floating lattice", in which an energy gain by the vortex lattice formation dominates over that by the vortex core pinning. As shown in Fig. 3(b), the QPI pattern in the floating lattice is almost regarded as a sum of QPI's in the first and second cases.

Here, let us move each impurity site into the vortex core in order to create the so-called "pinned lattice". In this case, we find that the calculated Free energy is reduced compared to that of floating lattice. As the fourth case, we move an impurity marked by the red line circle in Fig. 3(a) to the marked vortex core as shown in Fig. 3(c). Then, the marked vortex of Fig. 3(c) is assigned to "pinned vortex", and the QPI in the presence of the pinned vortex is displayed in Fig. 3(d). By comparing Fig. 3(d) with Fig. 3(b), one finds that intensified points are located close to $\mathbf{q}_1 = (\pi, 0)$, $\mathbf{q}_2 \sim (2.3, 2.3)$ and $\mathbf{q}_3 \sim (1.2, \pi)$. As these \mathbf{q} 's are displayed in the left panel of Fig. 4, \mathbf{q}_1 , \mathbf{q}_2 and \mathbf{q}_3 , correspond to the scattering vectors represented by $\mathbf{k}_F^f(0) - \mathbf{k}_F^i(\pi)$, $\mathbf{k}_F^f(\pi/4) - \mathbf{k}_F^i(5\pi/4)$, and $\mathbf{k}_F^f(3\pi/8) - \mathbf{k}_F^i(11\pi/8)$, respectively, where $\mathbf{k}_F^f(\theta)$ and $\mathbf{k}_F^i(\theta)$ are the Fermi wave vectors after and before the scattering, and θ denotes the position angle on the Fermi surface. One can find that \mathbf{q}_1 and \mathbf{q}_3 vectors mean sign-preserving scatterings. On the other hand, one notices for \mathbf{q}_2 -vector that one needs a numerical check in judging whether \mathbf{q}_2 really corresponds to a sign-preserving scattering or not. The result is displayed in the right

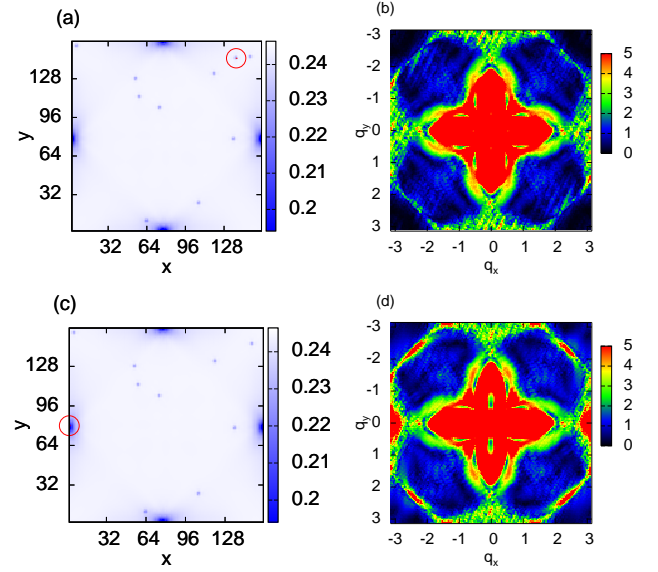


FIG. 3. (Color online) (a) and (c): Spatial profiles of the $d_{x^2-y^2}$ -wave order-parameter amplitude $|\Delta_d(\mathbf{r}_i)|$. (b) and (d): \mathbf{q} -space profiles of $Z(\mathbf{q}, E)$. For the definition $Z(\mathbf{q}, E)$, see the caption of Fig. 1. We consider the 160×160 square lattice system with 10 randomly distributed impurities with vortices. (a) and (b): Any impurities are not located inside vortices ("unpinned vortex"). (c) and (d): One impurity is located inside a vortex ("pinned vortex").

panel of Fig. 4, which distinguishes the sign-preserving with the reversing one in \mathbf{q} -space quadrant by actually examining \mathbf{q} -vectors around the Fermi surface ($\pm 0.1t$). From the right panel of Fig. 4, it is found that \mathbf{q}_2 is also a sign-preserving vector. These facts indicate that the sign-preserving scatterings are intensified by the emergence of the pinned vortex core. In addition, we should note that the vortex arrangement influenced by the vortex pinning is not important for QPI phenomena, since these origins are localized near a vortex-core and an impurity. We also note that these QPI phenomena are not originated from the disordered effects since we put only ten impurities whose density is 0.04% in our system, which can be assigned as a dilute-impurity doped case. In reality, the number of pinned vortex cores increases when increasing the magnetic field. Then, one can expect that only the sign-preserving \mathbf{q} -points grow in the QPI pattern. We emphasize that it is consistent with the measurement results. The presence of pinned vortices is essential for the phase sensitive detection of the superconducting order parameter. Indeed, such sign-preserving scattering peaks are non-observable in too clean sample²⁰.

IV. DISCUSSION

Finally, let us discuss the present numerical scheme and the obtained QPI results. The first issue is an advan-

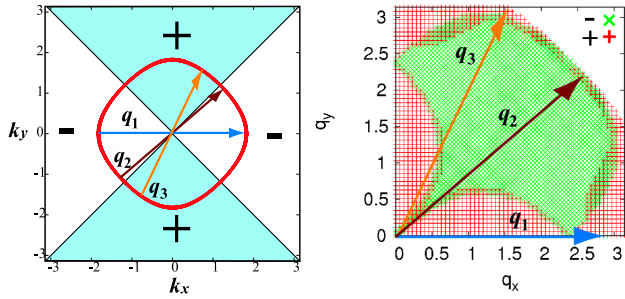


FIG. 4. (Color online) Left panel: A \mathbf{k} -space profile of the Fermi surface (red solid curve) in the square lattice model with $\mu = -1.5t$ and the white and shaded areas represent signs of d -wave superconducting gap on \mathbf{k} -space. The arrows denote typical sign-preserving scattering \mathbf{q} -vectors (See the text). Right panel: A \mathbf{q} -space profile of the sign preserving (+) and reversing (-) on the superconducting gap.

tage of the Chebyshev-polynomial expansion scheme in self-consistently calculating the BdG equations. In order to obtain a QPI map by Fourier transforming a real-space conductance map, one needs to solve the BdG equations on a sufficiently large real-space. Thus, there has been so far no study to directly calculate QPI's. This clearly indicates that the conventional diagonalization scheme is never a practical way in studies like the present topic and an alternative more efficient scheme is demanded. Very recently, Covaci *et al.*, have proposed a quite efficient scheme based on the Chebyshev-polynomial expansion to examine inhomogeneous superconductivity¹⁵. The main idea is an expansion of the Green's function by a set of Chebyshev-polynomials, which guarantees a drastic reduction of the calculation cost. However, Covaci *et al.*, left a self-consistent calculation as the future work. Thus, the present work is the first self-consistent large-scale BdG calculation including the vector potential. We confirm in the present case that the computational cost totally scales with $\mathcal{O}(N^2)$ on the real-space grid size N and find that the number of the self-consistent iterations is almost equivalent with that in the matrix diagonalization. This means that the calculation cost is reduced to $\sim 1/N$ compared to the diagonalization scheme. Moreover, we developed several techniques in order to accelerate the calculation (see Ref.¹⁸ for the details). The second issue is an origin of the present QPI pattern in the presence of the pinned vortex. Previously, the resonant Andreev scattering has been regarded as the scattering

mechanism around a vortex^{9,10}. However, our numerical calculations reveal that the spatial variation of the order parameter induced by a vortex does not work as an effective scatter. In fact, as seen in Fig. 2, we can not find out any characteristic wave-vector peaks unlike the typical QPI map as Fig. 1. Thus, the QPI origin of the pinned lattice is explained as follows. The Andreev bound states around a vortex core are slightly distorted by impurity inside the vortex core²¹. A set of such distorted states scatter quasi-particles like an impurity while still keeps the angular momentum breaking the time reversal symmetry. Thus, we easily notice that a pinned vortex becomes a sign-preserving scatter and the number of such scatters increases with increasing the magnetic field. On the other hand, the number of the sign non-preserving scatter contrarily decreases with increasing the magnetic field, since the number of the scalar impurities outside the vortex core decreases with increasing the magnetic field. These consequences are consistent with the experimental results. In addition, our discussion can be easily applicable to the iron-based superconductors², since the present above scenario is considered to be also kept in multi-band superconductors. The realistic calculation for iron-based superconductors is a future work.

V. CONCLUSION

In conclusion, we self-consistently performed large-scale BdG calculations in the presence of vortices together with random impurities by using the Chebyshev-polynomial expansion scheme to investigate QPI in the magnetic field. Our calculations concluded that the a vortex core distorted by impurity works as an impurity breaking the time reversal symmetry. The microscopic finding well explains the observed experimental data, e.g., the QPI peaks relevant to the sign-preserving quasi-particle scattering grows while the sign-reversing one diminishes with increasing the magnetic field. Our direct calculations confirmed that the magnetic field dependence of QPI is a true phase-sensitive tool for unconventional superconductors.

We would like to thank Y. Ota and R. Igarashi for helpful discussions. The calculations have been performed using the supercomputing system PRIMERGY BX900 in Japan Atomic Energy Agency.

REFERENCES

- ¹ C. C. Tsuei and J. R. Kirtley, Rev. Mod. Phys. **72**, 969 (2000).
- ² T. Hanaguri, S. Nittaka, K. Kuroki, and H. Takagi, Science **328**, 474 (2010).
- ³ J. E. Hoffman, K. McElroy, D.-H. Lee, K. M. Lang, H. Eisaki, S. Uchida, and J. C. Davis, Science **297** 1148 (2002).
- ⁴ K. McElroy, R. W. Simmonds, J. E. Hoffman, D.-H. Lee,

- J. Orenstein, H. Eisaki, S. Uchida, and J. C. Davis, *Nature* (London) **422**, 592 (2003).
- ⁵ T. Hanaguri, Y. Kohsaka, J. C. Davis, C. Lupien, I. Yamada, M. Azuma, M. Takano, K. Ohishi, M. Ono, and H. Takagi, *Nat. Phys.* **3**, 865 (2007).
 - ⁶ Y. Kohsaka, C. Taylor, P. Wahl, A. Schmidt, J. Lee, K. Fujita, J. W. Alldredge, K. McElroy, J. Lee, H. Eisaki, S. Uchida, D.-H. Lee, and J. C. Davis, *Nature* (London) **454**, 1072 (2008).
 - ⁷ T. Hanaguri, Y. Kohsaka, M. Ono, M. Maltseva, P. Coleman, I. Yamada, M. Azuma, M. Takano, K. Ohishi, and H. Takagi, *Science* **323**, 923 (2009).
 - ⁸ T. Pereg-Barnea and M. Franz, *Phys. Rev. B* **78**, 020509(R) (2008).
 - ⁹ M. Maltseva and P. Coleman, *Phys. Rev. B* **80**, 144514 (2009).
 - ¹⁰ Tamara S. Nunner, Wei Chen, Brian M. Andersen, Ashot Melikyan, and P. J. Hirschfeld, *Phys. Rev. B* **73**, 104511 (2006).
 - ¹¹ Y. Y. Zhang, C. Fang, X. Zhou, K. Seo, W.-F. Tsai, B. A. Bernevig and J. Hu, *Phys. Rev. B* **80**, 094528 (2009).
 - ¹² Y. Nagai and Y. Kato, *Phys. Rev. B* **82**, 174507 (2010).
 - ¹³ A. V. Balatsky, I. Vekhter, J.-X. Zhu, *Rev. Mod. Phys.* **78**, 373(2006)
 - ¹⁴ Y. Wang, A. H. MacDonald, *Phys. Rev. B* **52** (1995) 3876(R).
 - ¹⁵ L. Covaci, F. M. Peeters, and M. Berciu, *Phys. Rev. Lett.* **105**, 167006 (2010).
 - ¹⁶ W. Kunishima, M. Itoh, and H. Tanaka, *Prog. Theo. Phys. Supplement* **138**, 149 (2000).
 - ¹⁷ H. Tanaka, W. Kunishima, M. Itoh, *RIKEN Review* **29**, 20 (2000).
 - ¹⁸ Y. Nagai, Y. Ota, and M. Machida, *J. Phys. Soc. Jpn.* **81** (2012) 024710.
 - ¹⁹ M. Takigawa, M. Ichioka, and K. Machida, *J. Phys. Soc. Jpn.* **69**, 3943 (2000).
 - ²⁰ T. Hanaguri, private communication.
 - ²¹ Such distortion is too subtle to observe in real-space DOS's, while observable as spots in the Fourier QPI map.